Available online at www.sciencedirect.com
ScienceDirect
Acta Materialia 58 (2010) 1876–1886
Acta MATERIALIA
www.elsevier.com/locate/actamat

The mechanical size effect as a mean-field breakdown phenomenon: Example of microscale single crystal beam bending

Eralp Demir, Dierk Raabe *, Franz Roters

Max-Planck-Institut für Eisenforschung, Max-Planck Str. 1, 40237 Düsseldorf, Germany

Received 14 May 2009; received in revised form 21 November 2009; accepted 21 November 2009
Available online 21 December 2009

Abstract

Single crystalline copper beams with thicknesses between 0.7 and 5 μm are manufactured with a focused ion beam technique and bent in a nanoindenter. The yield strengths of the beams show a mechanical size effect (smaller-is-stronger). The geometrically necessary dislocation (GND) densities estimated from misorientation maps do not explain the observed size effect. Also, accumulation of GNDs principally requires pre-straining. We hence introduce a mean-field breakdown theory and generalize it to small-scale mechanical tests other than bending. The mean-field breakdown limit is defined in terms of a microstructural correlation measure (characteristic dislocation bow-out length) below which the local availability of dislocation sources and not the density of GNDs dominates the mechanical size effect. This explains why a size dependence can occur for samples that are not pre-strained (by using a very small critical strain to define the yield strength). After pre-straining, when GNDs build up, they can contribute to the flow stress. The mean-field breakdown theory can also explain the large scatter typically observed in small-scale mechanical tests as the availability of sufficiently soft sources at scales around or below the correlation length does not follow statistical laws but highly depends on the position where the probe is taken.
© 2009 Acta Materialia Inc. Published by Elsevier Ltd. All rights reserved.

Keywords: Size effect; Electron backscattering diffraction (EBSD); Bending; Copper; Crystal plasticity

1. Introduction

As current trends towards device miniaturization accelerate, the micromechanical characterization of materials becomes increasingly important. Mechanical properties and the underlying plasticity mechanisms at dimensions below 20 μm differ from those at the macroscopic scale (smaller-is-stronger) [1–12]. Often, an inverse relationship is observed between the sample size and the flow stress. This applies even for compression tests under gradient-free loading conditions [13–15].

Mechanical tests at the microscale and macroscales are not only characterized by their sensitivity with respect to the initial microstructure and specific size-dependent deformation mechanisms (intrinsic size effects) but also by an increasing relative influence of the experimental initial and boundary conditions on the results (extrinsic size effects). The latter point has been discussed in terms of sample shape variations, contact, loading procedures and appropriate criteria to define the onset of plastic flow when comparing results obtained from samples of different size [8–10,16–23].

Intrinsic (microstructural) effects that are typically held responsible for the smaller-is-stronger phenomenon are geometrically necessary dislocations (GNDs) and pile-up effects [24]; dislocation starvation [12,25–27]; dislocation source truncation [28–32]; and changes in the dislocation forest [33]. The scaling of the yield stress with the probe size is different for these mechanisms. While GND-related strengthening leads to power-law exponents close to −0.5, source limitation effects show an exponent close to −1 [31]. As will be discussed below, these models all assume a mean-field behavior of the dislocations. Plastic deformation below the statistical regime (mean-field breakdown), however, is characterized by substantial deviations from

* Corresponding author. Tel.: +49 211 6792 333.
E-mail address: d.raabe@mpie.de (D. Raabe).

1359-6454/$36.00 © 2009 Acta Materialia Inc. Published by Elsevier Ltd. All rights reserved.
doi:10.1016/j.actamat.2009.11.031

the average dislocation behavior, and hence by large scatter of the observed flow stress values. This makes it difficult to fit corresponding data by one exponent alone and by that assign one single mechanism to the observed size effect. The same argumentation applies when transitions between different deformation mechanisms take place in a sequence of smaller-is-stronger experiments. This can be particularly expected when probe sizes below and above characteristic microstructural length scales are used. As will be discussed later, these inner length scales are referred to here as correlation length [33]. A third problem in assigning a single exponent and/or mechanism to a set of yield strength data is the often quite arbitrary definition of the yield begin.

In order to cast these thoughts more consistently into a generalized interpretation of mechanical size effects, we first have to classify the different intrinsic mechanisms into two groups, namely: (i) GND-based concepts and (ii) dislocation source limitation and truncation effects.

1.1. GND-based concepts

Strain gradient models attribute the inverse relationship between sample size and flow stress (or hardness) in micrometer dimensions to an increase in the GND density that is required to accommodate the lattice mismatch arising from second-order deformation gradients [24,25]. In a mean-field approximation these defects add to the overall dislocation density and, hence, strengthen the material according to Taylor's law

$$\tau^a = cGb\sqrt{\rho^a_{gnd} + \rho^a_{ssd}} \tag{1}$$

where c is a geometrical constant between 0.1 and 0.5, G is the shear modulus, b is the magnitude of the Burgers vector and ρ^a_{gnd}, ρ^a_{ssd} and τ^a are the geometrically necessary and statistically stored dislocation densities, and the yield strength on the slip system a, respectively. The strain gradient theory is often used to explain the indentation size effect (ISE) [24,25]. In this concept smaller probes are assumed to create larger strain gradients, which implies that the GNDs are confined to smaller volumes underneath the indents, leading to a larger flow stress [1].

In contrast to this model of size-dependent plasticity, recent experimental and theoretical works report about mechanical size effects under well-controlled deformation conditions in cases without externally imposed strain gradients or insufficient densities of GNDs, respectively [12,20–22,25,27,32,31,34–36]. These works suggest dislocation source limitation criteria as an alternative explanation for the size effect as outlined in (ii).

Another, more fundamental reason why GND-based theories cannot always explain size effects plausibly is that their accumulation requires an initial amount of pre-straining or thermomechanical treatment as in-grown dislocations at the onset of straining are not polarized (except in perlite or martensite). When measuring the yield strength after little or no pre-straining, GNDs cannot build up, and hence do not contribute to the size effect. Indeed, recent results in this field suggest that GNDs can cause a size effect of strain hardening rather than of the yield strength.

1.2. Dislocation source limitation and truncation effects

The second group of approaches to explain the smaller-is-stronger phenomenon considers dislocation slip and multiplication mechanisms that become size-dependent when the probe size becomes smaller than the microstructure correlation length [33]. These models explain the smaller-is-stronger effect without the presence of increased GND densities at smaller scales. The correlation length ξ is defined here as the most frequently occurring dislocation segment length between two pinning points that can potentially act as a dislocation source. It can be related to the inverse square root of the dislocation density (Taylor configuration), half the dislocation cell size or the average spacing of hard junctions. For the analysis of the yield stress size dependence at probe scales below that correlation length, statistical assumptions on the distribution and availability of potential dislocation sources do no longer apply. We refer to this situation as a mean-field breakdown regime. Three types of phenomena have been considered to be relevant for size effects in or close to that regime: dislocation starvation (exhaustion); dislocation source limitation or, respectively, truncation; and forest dislocation changes.

Dislocation exhaustion was primarily discussed for pillar compression [12,25,27]. It refers to a situation, where the smaller-is-stronger phenomenon of compressed crystals is associated with the depletion of mobile dislocations that leave the probed volume before multiplication can replenish the dislocation flux that is required to match an imposed shape change [26,29,37–40].

The dislocation source limitation or, respectively, source truncation effect refers to a situation, where, in confined geometries, only a limited number of potential (i.e. sufficiently soft) dislocation sources are available [9,10,29,31,41]. The source-operation stress is related to the dislocation arrangement. As the activation stress for Frank–Read sources scales inversely with the spacing of the pinning points, a mechanical size effect occurs if the softest sources (largest pinning length) in smaller samples become necessarily more narrow and, hence, harder to activate. This case is simply a generalization of the dislocation starvation mechanism because the main point about dislocation depletion is not that the existing dislocations leave the sample through the surface but that an insufficient number of sources are available to replenish the flux required to comply with the imposed boundary conditions.

A third aspect describes changes in the forest dislocation arrangement. The dislocation forest can act on size effects in two ways. First, potential dislocation sources are an inherent part of the forest arrangement. This establishes a relationship between the correlation length valid for a spe-

cific dislocation arrangement that is being probed and the softest available dislocation source length within this arrangement. Secondly, the dislocation forest acts through conventional effects, such as elastic interaction, cutting and reactions among dislocations in the ensemble when slip occurs.

These three groups of mechanisms thus have in common that the limitation in the dislocation multiplication rate through an insufficient availability of soft sources is the dominant factor for the smaller-is-stronger effect. This phenomenon can be expressed in terms of the Orowan equation [30,42–44]: when crystals are plastically loaded, dislocations glide and multiply following the locally acting shear stresses under the constraint of matching the imposed velocity gradient,

$$\dot{\gamma} = \rho_m b v + \dot{\rho}_m^+ b l \tag{2}$$

where ρ_m is the density of existing mobile dislocations, $\dot{\rho}_m^+$ is the rate of dislocation multiplication, l is the mean free path and v is the dislocation velocity. The first term in this equation represents the shear resulting from the expansion of existing dislocation loops and the second one accounts for the generation of new mobile dislocations.

Usually in bulk crystal plasticity Orowan's equation is not written as a total differential (as is done here). The reasons for usually dropping the multiplication term are that, first, it does not directly contribute to the shear, and secondly, a sufficient number of critical bow-out and source configurations are usually available in a mean-field approximation [43,44]. In bulk plasticity this assumption is justifiable as the Taylor stress scales with the square root of the dislocation density and so does the bow-out stress for a source when the pinning points are of the same order of magnitude as the mean dislocation spacing. However, in confined probe geometries, it is possible that multiplication rates are not high enough to maintain an imposed shear rate as the source activation stress scales inversely with size [27,45–48]. The Orowan equation as written here, therefore, maps the kinematic necessity that an imposed velocity gradient (here in scalar formulation) must be accomplished by dislocation slip, which has to be permanently replenished by a limited set of sources in the case of small samples.

In order to study these two different approaches (GNDs vs. mean-field breakdown) to explaining the smaller-is-stronger phenomenon in more detail, we investigate the size effect in terms of bending experiments. Bending is a good alternative to compression and indentation [6–11]. Stölken and Evans [6] observed stronger behavior of thinner Ni polycrystal thin films during bending for the same surface strain and reported size-dependent strength and strain hardening. Similarly, flow stresses up to 1 GPa were found for copper single crystal bending beams with 1 μm thickness by Motz and co-workers [9]. They used the maximum forces for calculating the yield stresses. The inverse thickness dependence of the yield strength was related to the existence of GNDs, together with piling-up of dislocations around the neutral axis of the beams. Corresponding observations were studied by using 3-D discrete dislocation dynamics simulations [10]. In that work, the GND densities were estimated from electron backscattered diffusion (EBSD)-derived kernel average misorientation (KAM)[1] maps [9,21] Eq. (3), where ω is the angular rotation over the distance x along the beam.

$$\rho_{gnd} = \frac{\omega}{x}\frac{1}{b} \tag{3}$$

In this work, cantilever beams of different dimensions were bent. Samples were manufactured by focused ion beam (FIB) milling and the beams were deformed with a spherical diamond tool in a nanoindenter while the forces were recorded. The GND densities were calculated using ex situ EBSD measurements of the lattice curvature in the cross-sections of the deformed beams. As the so-determined GNDs can only explain a minor portion of the observed size dependence (depending on the definition of yield begin), we discuss the results in terms of a generalized mean-field breakdown concept, as indicated above. This interpretation of the smaller-is-stronger effect is based on dislocation multiplication limitation and the availability of new sources as a function of the sample size in cases, where the probed volume is close to or even below the microstructure correlation length.

2. Experimental

Copper single crystals were grown in a Bridgman furnace. Beams were cut and a 3 μm layer was removed by FIB milling from the top and the side surfaces using high FIB currents (30 keV, 2–5 nA). The remaining cuts were made at decreasing currents using 500 pA for surface finishing. Finally, the side surfaces were cleaned using 100 pA prior to EBSD characterization. FIB machining tolerance was improved by several means. For instance, a tapered structure was typically formed when the beam was machined along the width of the sample. This initial taper was reduced by tilting the sample by 1.5° with respect to the FIB milling axis before cutting. In addition, a fast milling strategy (1 $\mu m^2\,s^{-1}$) for small incidence angle variation together with low milling currents (500 pA) was used to manufacture the finest structures. From these single crystals we manufactured cantilever beams with thicknesses between 0.7 and 5 μm via FIB milling (Fig. 1). All other beam dimensions were fixed ratios of their thickness (see the schematic drawing in Fig. 1, Table 1). The symbols w, t_{int}, t_{ext}, L, $y_{exerted}$ and $y_{measured}$ represent the width, interior thickness, exterior thickness, length, exerted moment arms and measured moment arms, respectively. The measured moment arm, $y_{measured}$, refers to the values determined from the scanning electron microscopy (SEM)

[1] Kernel average misorientation is a measure of the average misorientation between a given data point and its neighbors (excluding misorientations higher than some prescribed value).

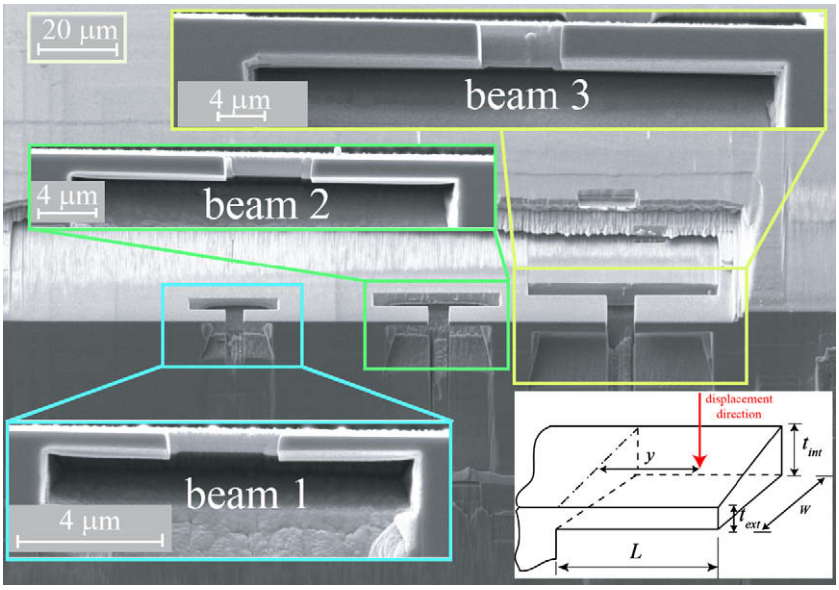

Fig. 1. SEM images of three cantilever beams with different thickness from the oblique and transverse views. The schematic drawing shows the beam geometry and naming convention. The symbols w, t_{int}, t_{ext}, L, $y_{exerted}$ and $y_{measured}$ refer to the width, interior thickness, exterior thickness, length, exerted moment arms and measured moment arms, respectively, as determined by SEM.

Table 1
Beam dimensions in μm (see also Fig. 1). The symbols w, t_{int}, t_{ext}, L, $y_{exerted}$ and $y_{measured}$ represent the width, interior thickness, exterior thickness, length, exerted moment arms and measured moment arms, respectively. The measured moment arm, $y_{measured}$, refers to the values determined from the SEM images after deformation.

	Beam 1a	Beam 1b	Beam 2a	Beam 2b	Beam 3a	Beam 3b
w (μm)	4.8	4.8	6.8	6.8	11.7	11.7
t_{int} (μm)	1.5	1.5	2.2	2.2	5.3	5.3
t_{ext} (μm)	0.6	0.6	1.2	1.3	3.2	3.2
L (μm)	5.9	7.3	10.3	10.6	19.2	20.5
$y_{exerted}$ (μm)	4.0	4.0	8.0	8.0	16.0	16.0
$y_{measured}$ (μm)	4.9	3.6	9.4	9.4	18.5	17.1

images after deformation. The exerted moment arm, $y_{exerted}$, refers to the values measured directly during bending via the indenter device optics. The difference in these two measures is analyzed in order to estimate possible positioning and alignment deviations between tool and beam. Orientation maps were taken using high-resolution EBSD in a field-emission scanning electron microscope (Fig. 2). We determined the Schmid factors from the orientations and boundary conditions (Table 2).

The samples were bent in a hysitron triboscope indenter. Total displacements of 0.5, 1 and 2 μm were imposed in dis-

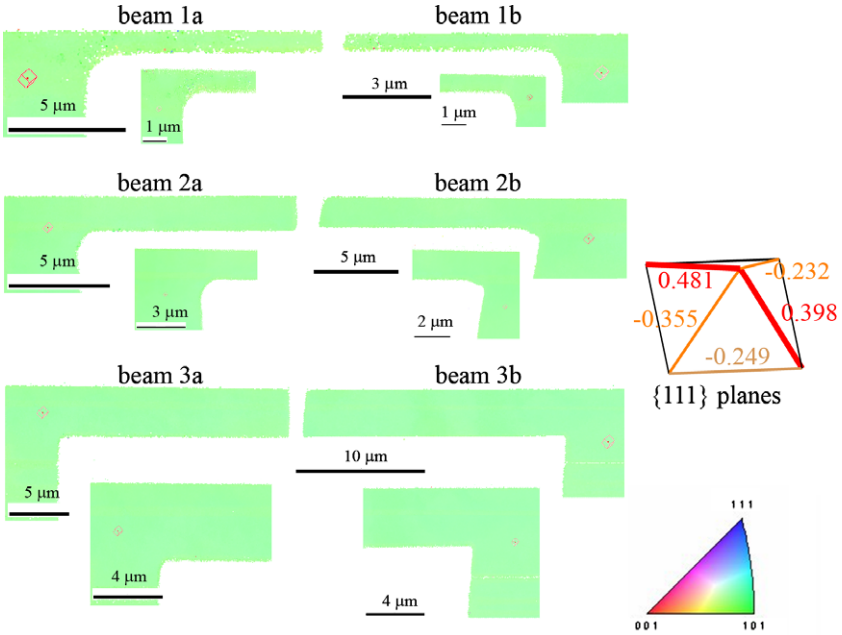

Fig. 2. Inverse pole figure maps of the beams before loading. The smaller figures are high-resolution EBSD close-up maps of the transition region between the beams and the bulk.

Table 2
Slip directions, slip planes and the corresponding Schmid factors.

Slip plane, $\vec{n}$	(1 1 1)			$(\bar{1}\,\bar{1}\,1)$			$(\bar{1}\,1\,1)$			$(1\,\bar{1}\,1)$		
Slip direction, $\vec{b}$	$[0\,1\,\bar{1}]$	$[\bar{1}\,0\,1]$	$[1\,\bar{1}\,0]$	$[0\,\bar{1}\,\bar{1}]$	$[1\,0\,1]$	$[\bar{1}\,1\,0]$	$[0\,1\,\bar{1}]$	$[1\,0\,1]$	$[\bar{1}\,\bar{1}\,0]$	$[0\,\bar{1}\,\bar{1}]$	$[\bar{1}\,0\,1]$	$[1\,1\,0]$
Schmid factor	**0.481**	**−0.355**	−0.126	**0.398**	**−0.232**	−0.166	0.032	0.012	−0.043	0.115	0.134	**−0.249**

placement control mode, respectively, as a function of the beam thickness to realize identical strain rates. The displacement was exerted as a sequence of 10 subsequent loading and five unloading steps for a duration of 10 s for each loading and unloading step. The dwell time between loading and unloading steps was 5 s. The loading rates corresponded to a strain rate of approximately 0.025 s^{-1} in all cases. A conical diamond indenter with a spherical tip was used to make the indentations (5 μm tip radius, Hys-Ti45).

3. Results and discussion

We observed dislocation slip traces with a thickness of ≈40–50 nm on the surfaces of the beams. They became more pronounced with increasing beam thickness. Slip traces are shear steps, hence they reveal areas of pronounced dislocation activity and shear localization. Similar information was retrieved from the KAM maps of the bent beams (the corresponding orientation maps were measured

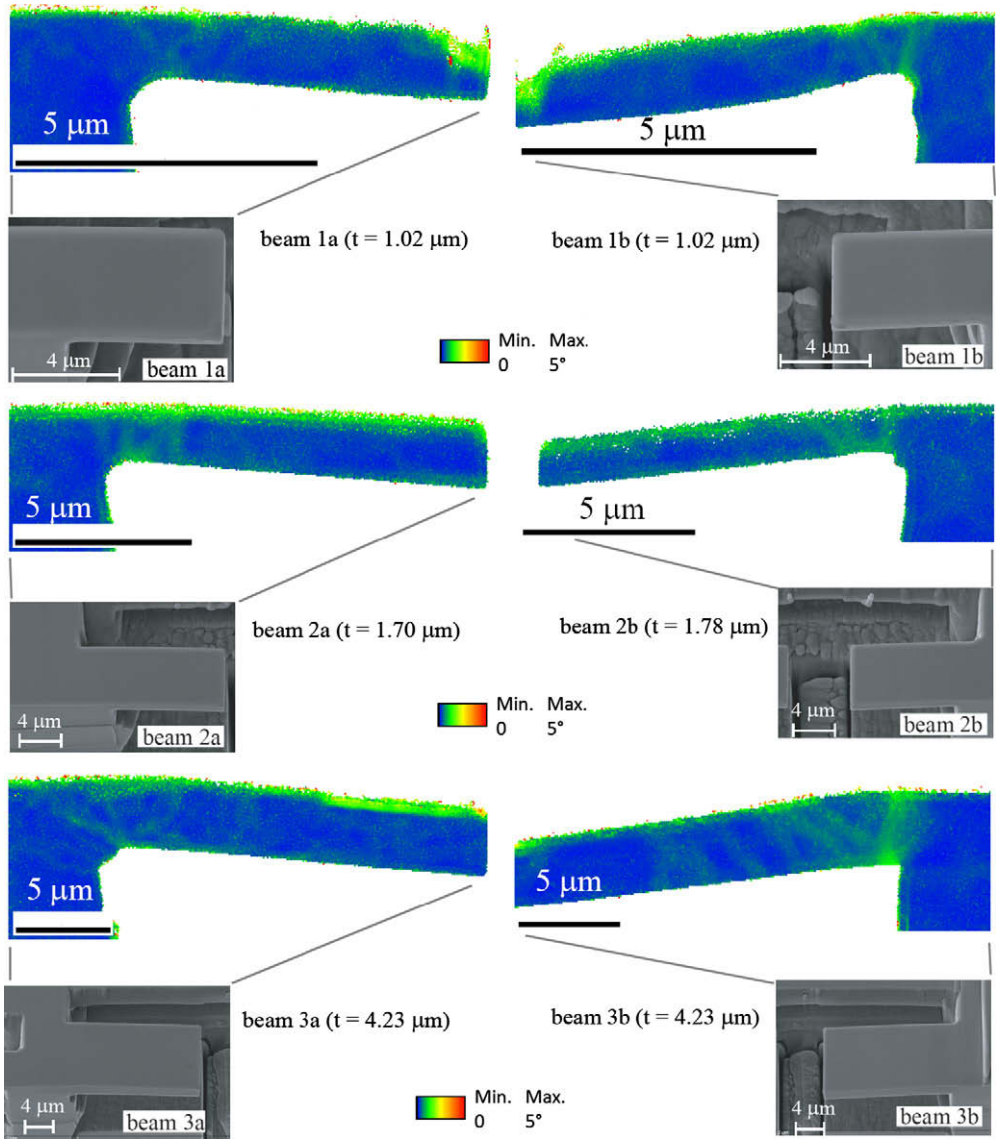

Fig. 3. SEM images after bending at a 70° tilt position for EBSD characterization together with the corresponding KAMs of the side sections. The KAM value in this case is an averaged misorientation measure using the first, second and third nearest neighbor orientation shells. The confidence index was higher than 0.1. The confidence index is the difference between the first and second highest ranked orientation solutions. A confidence index above 0.1 means that 95% of the crystallographic indexing was correct.

Table 3
Average thickness, GNDs approximated from the measured EBSD misorientations and the corresponding KAM measure at the end of bending deformation Eq. (3), mean GND spacing and total rotation angle of the beams.

	Average thickness (μm)	GND ($1/m^2$)	Mean spacing (nm)	Total rotation (deg)
Beam 1a	1.02	9.58×10^{13}	100	2.61 ± 0.31
Beam 1b	1.02	2.21×10^{14}	70	6.35 ± 0.49
Beam 2a	1.70	8.26×10^{13}	110	4.21 ± 0.19
Beam 2b	1.78	1.04×10^{14}	98	4.53 ± 0.11
Beam 3a	4.23	3.08×10^{13}	180	4.10 ± 0.54
Beam 3b	4.23	5.44×10^{13}	135	5.66 ± 0.27

ex situ after plastic bending) (Fig. 3). They reveal local orientation gradients, and were used to estimate the GND densities using Eq. (3) (Table 3). The KAM maps have the following features. (i) The orientation changes are not homogeneous but they form localized patterns originating particularly at the transition zones between the beams and the bulk material. In these regions 3-D stress concentrations prevail. This suggests that deformation occurs in the form of localized shear zones rather than as ideal homogeneous bending. (ii) The misorientations at the top and the bottom parts of the beams are not identical (as would be expected for ideal bending) owing to the non-symmetrical influence of the curvature at the connection between the beam and the bulk material. (iii) Orientation changes initiate from those points, where the applied stress is highest during bending.

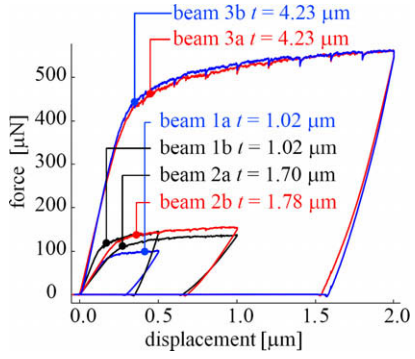

Fig. 4. Force–displacement curves of the beams.

Fig. 4 shows the force–displacement curves for the beams. The variation in the elastic stiffness is due to the variation in the moment arms among the different beams. The flow stresses are calculated from the force–displacement curves using Eq. (4), in which F, y, w_{sum} and t_{av} refer to the forces, moment arms, width and average thickness of the beams, respectively (Fig. 1).

$$\sigma = \frac{4Fy}{w_{sum}t_{av}^2} \tag{4}$$

Fig. 5 shows the bending stress–strain (a) and the strain hardening (Θ) diagrams (b). The stresses are calculated according to Eq. (4) after normalizing the displacements by the corresponding moment arms. As a strain measure we use the d/y ratio. d, F, y, w_{sum} and t_{av} refer to the displacement, force, moment arm, beam width and average beam thickness, respectively. Although normalization of the displacements does not yield the exact strains (as the beams were not bent around the same well-defined curvature radius), the match in the elastic stiffness among the different beams shows that the moment arm is a reasonable normalization measure.

Fig. 6 shows the yield strength data obtained from the corrected and normalized stress–strain curves given in

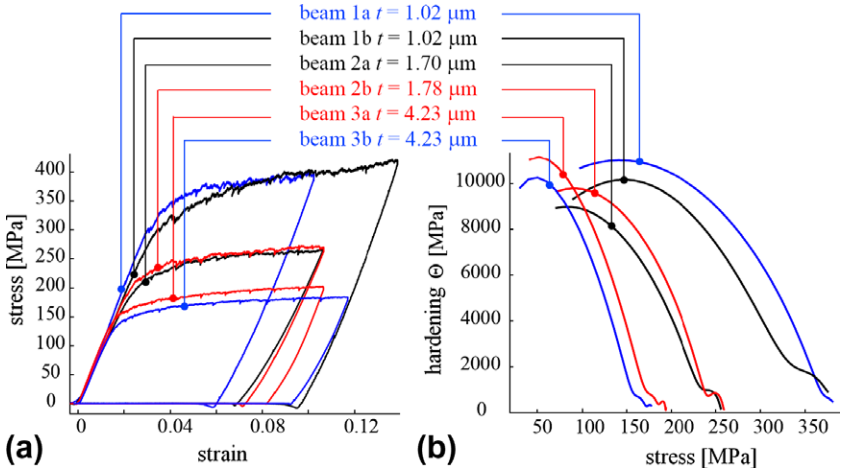

Fig. 5. (a) Stress–strain and (b) Kocks–Mecking-type strain hardening diagrams. The bending stress σ is calculated using $4Fy/w_{sum}\,t_{av}^2$ Eq. (4). As a strain measure we use the d/y ratio. d, F, y, w_{sum} and t_{av} refer to the displacement, force, moment arm, beam width and average beam thickness, respectively.

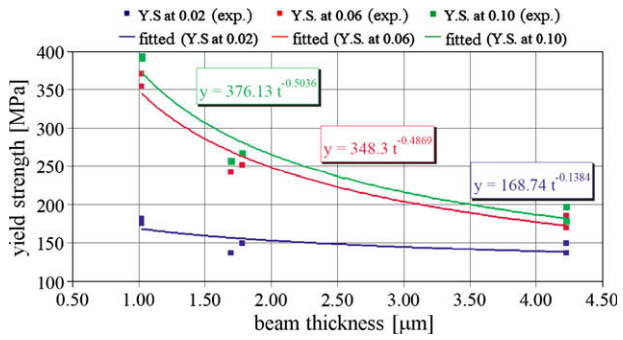

Fig. 6. Yield strength vs. beam thickness obtained from the stress–strain curves (Fig. 5) by using three different yield criteria (0.02, 0.06 and 0.10 strain). Y.S. refers to the yield strength.

Fig. 5 as a function of the beam thickness using three different yield criteria (0.02, 0.06 and 0.10 strain). The motivation for this analysis is to differentiate between the size dependence of the yield strength and the size dependence of the early stages of strain hardening (Fig. 5), as similarly discussed in Refs. [6,50]. The yield strength values obtained for a strain of 0.10 are slightly lower than those reported by Motz et al. for copper single crystals [9]. The reason for the deviation might be the initial orientation and the yield strength criterion used in Ref. [9], which was based on the maximum of the forces rather than on the critical strain.

Typical criteria for the onset of plastic yielding in previous works were, for instance, the maximum of the forces, a 0.2% strain threshold (or even considerably larger values) or the onset strains for necking. The stress values in Fig. 6 and their dependence on the experimental boundary conditions reveal that a crisp definition of the yield strength (and, hence, of its size dependence) is an essential point when interpreting small-scale experiments: when applying the lowest yield criterion to the current data (stress at 0.02 strain), the beams show a relatively weak mechanical size effect of the yield strength. It increases from 150 MPa for the largest beams (4.25 μm beam thickness) to about 180 MPa for the smallest beams (1 μm beam thickness). This corresponds to a size-related increase of 20% in yield strength upon probe refinement. In contrast, the highest yield criterion (stress at 0.1 strain) shows the strongest increase in strength upon size reduction (about 100%). The flow curves in Fig. 5a shows that at 0.1 corrected strain substantial plastic deformation has already occurred. This analysis documents that the use of a high strain value (0.1) as a more or less arbitrary threshold measure for the yield strength is not useful as it includes strain hardening effects [50]. It also shows that the yield stress is only weakly size-dependent when using a small strain criterion to define yield begin [50]. This is also evident from Fig. 5b, which shows that strain hardening is particularly pronounced in the incipient strain regime. Such behavior applies to practically all metals (outside the superplastic regime). Figs. 5b and 6 further reveal that strain hardening is also size-dependent, and that it decays drastically, particularly at the beginning of plastic yielding. This means that high strain threshold measures for defining yield begin are not suited for the definition of the yield stress as small changes in initial strain entail a large shift in the so-defined yield stress. Corresponding size effect analysis hence provides no information about the size dependence of the yield strength. Instead, it quantifies the joint size dependence of the yield strength and of strain harding. However, it does so only for a rather arbitrarily selected strain level. In contrast, the smallest chosen threshold strain (0.02) is also a critical measure for the definition of the yield strength (in the current case), as for some samples Fig. 5a suggests that plasticity is not yet percolative.

An interesting additional aspect can be concluded from the apparent size effect observed for the 0.06 and 0.1 strain data sets (Fig. 6). These two curves show an inverse square root yield strength dependence on the beam thickness. This observation indicates that the size dependence of the flow stress after an initial amount of pre-straining follows a GND-based theory (curves for 0.06 and 0.1 strain) while the initial yield strength after little or no pre-straining does not (see the curve for the 0.02 strain criterion). This conclusion is plausible as the accumulation of GNDs principally requires pre-deformation. Using GNDs to explain a size effect of undeformed samples is not conclusive as in-grown dislocations at the onset of staining are not polarized. Hence, when no such pre-straining is imposed (because a very small critical strain is selected to define the yield strength) the size dependence must be due to the availability of dislocation sources. This aspect will be discussed below in more detail.

The analysis shows that a more precise definition is required for the yield strength, particularly when analyzing mechanical size dependence. One approach might be the definition of Kocks, who referred to the yield strength as percolative plastic deformation, where the sheared area must penetrate the material portion under consideration [49]. This approach is not well suited for the field of small-scale plasticity, though, as it anticipates a mean-field approximation of plasticity and is not directly accessible to experimental characterization. In contrast, it has frequently been observed that plasticity occurs in microscale experiments in a highly localized fashion via sudden strain bursts and microbanding [12,25,27,29,37–39]. These observations suggest that a mean-field definition of percolative straining is not adequate in small-scale plasticity, which takes place essentially in or close to the mean-field breakdown regime. Another definition for the onset of yielding was suggested by Van Swygenhoven and co-workers, who used a change in the direction of the motion of the peaks during in situ white-light Laue diffraction experiments [50,51]. They also came to the conclusion that the large smaller-is-stronger effect reported in some previous works is due to the size dependence of strain hardening rather than to the size dependence of the yield strength.

Fig. 7 compares the experimentally observed to the calculated resolved shear stresses. The experimental data were derived by translating the resolved macroscopic bending stresses into the crystallographic shear stresses in the active slip systems using the Schmid factor for the primary slip system (0.481). The calculated data in the same diagram were derived from the misorientation measurements (Fig. 3) and the corresponding GNDs through Taylor's relationship Eq. (1), using a geometry factor (α), Burgers vector (b) and single crystal shear modulus (G) of 0.4, 0.255 nm and 53 GPa (anisotropy considered), respectively. The GND density values are shown in Table 3. As the underlying orientation maps, from which the GNDs were derived, could only be obtained ex situ after deformation, we compared the stresses (calculated, measured) at the end of plastic bending. Thus, this comparison does not help in analyzing the size effect but it is used as a consistency test between experiment and GND-based theory. The comparison reveals the following points. First, the strength data calculated by using the GND densities are in all cases smaller than the experimentally observed values (by a factor of 2.5–3 depending on beam thickness). Secondly, the scatter for each data set is much smaller than the difference between the GND-derived and the measured stresses. Thirdly, the weakness of this comparison is the fact that the statistically stored dislocation density was unknown and hence neglected in the stress calculation. The observations suggest that a gradient-based strengthening mechanism acting solely through additional GNDs cannot be solely responsible for the observed strength values.

This conclusion, together with the results discussed in Fig. 6, takes us back to the interpretation of the size effect in terms of a mean-field breakdown approach. It provides a statistical interpretation of the smaller-is-stronger phenomenon that is in good agreement with recent experimental observations [12,20–22,25,27,31,34–36,41] and theoretical considerations without using GNDs [41,52].

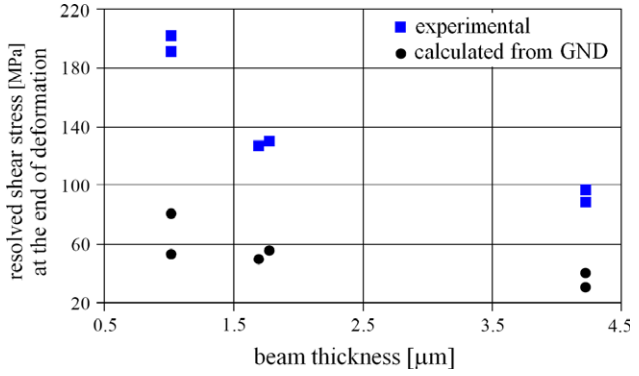

Fig. 7. Comparison of the measured resolved shear strength values to the calculated ones. The experimentally obtained resolved shear strength data were obtained by multiplying the values obtained from the stress–strain curves at the end of deformation shown in Fig. 5 with the corresponding Schmid factor of the primary slip system (0.481). The calculated resolved shear strength values were obtained from the local misorientation measurements and the resulting strength effect of the GND density (Fig. 5) at the end of deformation.

We assume as a starting point that in a micro or nano-sized samples the availability of soft dislocation sources is the main factor that can lead to an increase in flow stress upon size reduction [12,25,27,29,30,37–40]. In the mean-field breakdown theory we approximate this effect in terms of two size-dependent functions (Fig. 8). The first one is the activation stress for a dislocation source, which is a hyperbolic function of the bow-out segment length. This function represents the dislocation source strength at different available segment scales (top curve). It shows that in small-scale experiments the softest (i.e. largest) source is defined by the half probe (sample) size. The second function shows a typical probability distribution of dislocation segments that are potentially available as sources (bottom curve). The latter function has three characteristics: the minimum possible bow-out length is defined by the Burgers vector; the maximum value is the half sample or probe size; and between these two extreme values a pronounced maximum is likely to occur. This maximum is referred to as the correlation length ξ [33]. It is defined as the most frequently occurring potential bow-out segment length. It can be related to the inverse square root of the dislocation density in the case of a Taylor configuration, to half the dislocation cell size or to the average spacing of hard junctions. We give an estimate of the correlation lengths for the current experiments below. The exact shape of the dislocation source function is speculative to some extent, but its details are not vital for maintaining the mean-field breakdown approach with respect to the interpretation of the smaller-is-stronger effect.

If the mechanical probe size L exceeds the correlation length ξ, the experiment is conducted in the mean-field domain. This regime is characterized by a statistical distribution of sources and a high probability that the probed material contains a source. Also, the most probable source size (defined by the correlation length ξ) is always smaller than the sample size. For this reason the size effect in this regime is rather small, and should become less relevant the more the sample size exceeds the correlation length. The size effect should depend only weakly on the inherited microstructure (sample history) in this case. One should note, though, that the correlation length is a microstructure parameter and, hence, a history-dependent variable. This means that the same material will reveal a different correlation length and consequently a different transition size between the mean-field and mean-field breakdown regime when the microstructure is altered, e.g. by preceding plastic deformation or cyclic loading.

In contrast, if the probe size L is smaller than or of the same order as the correlation length ξ, the experiment that takes place is in the mean-field breakdown regime. This regime is characterized by considerable local fluctuations in the availability of potential sources. In this case, the most probable source is generally also the softest available source. The softest critical bow-out length is always identical to the half sample size. This relationship leads to a strong size effect in the mean-field breakdown regime. As

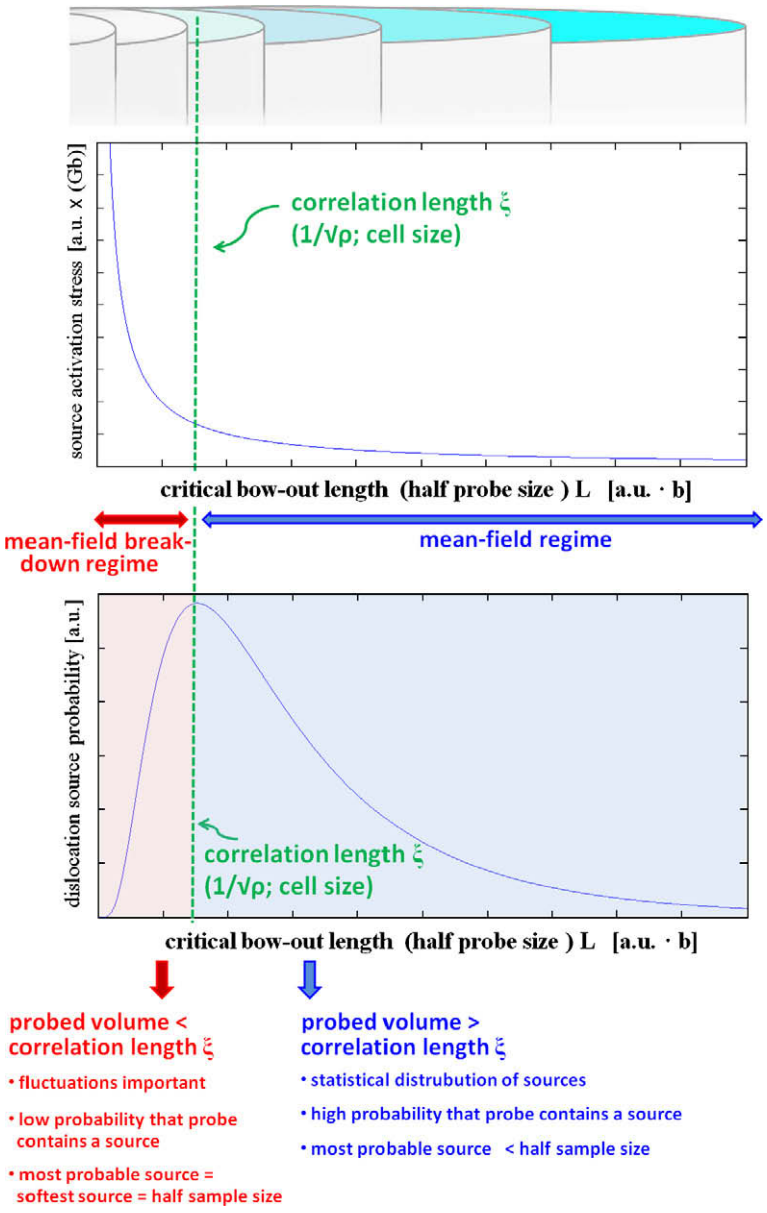

Fig. 8. Schematic presentation of the mean-field breakdown approach as a statistical interpretation of the mechanical size effect. The top row schematically indicates a set of probed volumes with increasing dimensions and decreasing mechanical size effect (smaller-is-stronger). The second row shows the dependence of the dislocation source strength in arbitrary units (a.u.) as a function of the critical bow-out length. In small-scale experimentation the softest (i.e. largest) source is defined by the half probe (sample) size. The third row shows a typical probability distribution of dislocation segments that are potentially available as sources. The correlation length ξ is the most frequently occurring potential bow-out configuration, usually given by the inverse square root of the dislocation density, the dislocation cell size or the average spacing of hard junctions. If the probe L is larger than the correlation length ξ the experiment is conducted in the mean-field regime; if it is smaller, the experiment is conducted in the mean-field breakdown regime.

the overall probability to encounter such a soft source, however, is very small, measurements in this regime necessarily show very large scatter and a strong dependence on the inherited microstructure.

In either case, the mean-field breakdown interpretation of the size effect is simply a generalization of the dislocation starvation mechanism because the main point of dislocation depletion is not that the existing dislocations leave the sample through the surface but that an insufficient number of sources are available to replenish the flux required to comply with the imposed boundary conditions.

We now apply the mean-field breakdown theory to our current experimental data. For this purpose we estimate the correlation length from the average initial dislocation density of the beams at yield begin using the data shown in Fig. 6 using the following approach. First, we select the stresses obtained for the smallest (0.02 strain, blue curve in Fig. 6)[2] and the highest yield criterion (0.1 strain, green curve in Fig. 6) to obtain an upper and a lower bound for

[2] For interpretation of color in Figs. 1–8, the reader is referred to the web version of this article.

the correlation length, respectively. Secondly, we select in either case only the yield strengths of the largest beams to make sure that the correlation length represents the bulk dislocation microstructure of the material in its mean-field state. This reflects the condition that the initial microstructure of an undeformed beam that is cut from a bulk single crystal does not know the size of the sample, provided that the beam size is larger than the correlation length. Thirdly, we use the Taylor equation (Eq. (1) in conjunction with a Taylor factor of 3 to extract the dislocation density of the largest beams for both cases and, from its inverse square root, the correlation length. The upper bound estimate yields a value of 0.35 μm (0.02 strain criterion for yield begin; largest beam in Fig. 6) and the lower bound estimate 0.26 μm (0.1 strain criterion for yield begin; largest beam in Fig. 6) for the correlation length. These values are very close to the dimensions of the smallest half-beam dimensions (0.51 μm half thickness). This means that, according to this simple approximation of the correlation length, the beams were deformed close to the transition regime between the mean-field and the mean-field breakdown regimes. We hence attribute the discrepancy between the experimentally observed smaller-is-stronger effect and the GND-related contribution (Fig. 7) to the mean-field breakdown effect (Fig. 8). More specifically, we suggest that the size dependence at the onset of straining is due to the availability of dislocation sources and the relationship between the dislocation correlation length and the probe size. After some pre-straining, when GNDs can build up during bending, they also contribute to the flow stress.

Another aspect that can be discussed in terms of the mean-field breakdown theory is the large scatter typically inherent in small-scale mechanical experiments. Plasticity in probed volumes that are smaller than the correlation length can only be explained in terms of the specific local discrete behavior of a very small set of dislocations that as a rule does not match the behavior of a statistical ensemble. As the dislocation substructure changes at different scales and under different loading and history conditions, so does the correlation length. This means that the correlation length, which acts as a potential critical bow-out radius required for multiplication, is a pronounced microstructure variable. When a probed volume is in the mean-field breakdown regime, the actual mechanical response depends on the discreteness of the local dislocation arrangement. At this scale, local details in the arrangement and corresponding spatial fluctuations start to play an important role on the size effect.

4. Conclusions

- We conducted microscale bending of single slip-oriented copper single crystal beams and subsequent EBSD characterization.
- Geometrical inaccuracies may significantly influence the resulting microstructure by causing stress concentrations. The effect of these inaccuracies on the microstructure can be mapped using EBSD.
- Plastic bending proceeds more in the form of localized shear events rather than as ideal bending.
- The measured flow strength values were size-dependent. The yield strengths varied not only with the beam thickness but also strongly with the yield criterion selected. Changing the threshold strain from 0.02 to 0.1 increased the flow stress values by 270% for the smallest beams. The reason for this effect is the size dependence of strain hardening. The analysis hence revealed that the contribution of strain hardening to the smaller-is-stronger phenomenon is more important than the incipient size dependence of the flow strength observed at the onset of plastic straining. From the size effect exponents we conclude that strain hardening during the early bending stages can be attributed to GNDs (see the yield strength data taken at 0.1 pre-deformation) while the actual yield strength at a strain of 0.02 (i.e. without substantial pre-deformation) is not due to GNDs.
- To fully understand the observed smaller-is-stronger effect we introduce a microstructural mean-field breakdown theory and generalized it to other small mechanical tests. The mean-field breakdown limit is defined by a microstructural correlation measure (characteristic bow-out length) below which the local availability of dislocation sources and not the density of GNDs determines the mechanical size effect. According to our estimates, the current bending experiments can be interpreted in terms of this theory. Moreover, the mean-field breakdown approach explains why a (weak) size dependence can indeed exist for samples that are not pre-strained. Accumulating GNDs principally requires pre-deformation. When no such pre-straining is imposed (because a very small critical strain is selected to define the yield strength), the size dependence is exclusively due to the availability of dislocation sources and the relationship between the dislocation correlation length and the probe size. After some pre-straining, when GNDs build up during bending, they also can contribute to the flow stress. The mean-field breakdown theory can also explain the large scatter typically observed in small-scale mechanical tests as the availability of sufficiently soft sources at scales around or below the correlation length does not follow statistical laws but is highly dependent on the position where the probe was placed.

References

[1] Fleck NA, Muller GM, Ashby MF, Hutchinson JW. Acta Metall 1994;42:475.
[2] Nix WD, Greer JR, Feng G, Lilleodden ET. Thin Solid Films 2007;515:3152.
[3] Uchic MD, Dimiduk DM. Mater Sci Eng 2005;400:268.
[4] Volkert CA, Lilleodden ET. Philos Mag 2006;86:5567.
[5] Uchic MD, Dimiduk DM, Wheeler R, Shade PA, Fraser HL. Scripta Mater 2006;54:759.

[6] Stölken JS, Evans AG. Acta Mater 1998;46:5109.
[7] He JH, Luo JK, Le HR, Moore DF. Mater Sci Eng 2006;423:134.
[8] Dehm G, Motz C, Scheu C, Clemens H, Mayrhofer PH, Mitterer C. Adv Eng Mater 2006;8:1033.
[9] Motz C, Schoberl T, Pippan R. Acta Mater 2005;53:4269.
[10] Motz C, Weygand D, Senger J, Gumbsch P. Acta Mater 2008;56:1942.
[11] Gong J, Wilkinson AJ. Acta Mater. 2009;57:5693.
[12] Greer JR, Nix WD. Phys Rev B 2006;73:245410.
[13] Uchic MD, Dimiduk DM, Florano JN, Nix WD. Science 2004;305:986.
[14] Benzerga AA, Shaver NF. Scripta Mater 2006;54:1937.
[15] Choi YS, Uchic MD, Parthasarathy TA, Dimiduk DM. Scripta Mater 2007;57:849.
[16] Raabe D, Ma D, Roters F. Acta Mater 2007;55:4567.
[17] Maass R, Van Petegem S, Zimmermann J, Borca CN, Van Swygenhoven H. Scripta Mater 2008;59:471.
[18] Zaafarani N, Raabe D, Roters F, Zaefferer S. Acta Mater 2008;56:31.
[19] Zaafarani N, Raabe D, Singh RN, Roters F, Zaefferer S. Acta Mater 2006;54:1863.
[20] Rester M, Motz C, Pippan R. Acta Mater 2007;55:6427.
[21] Demir E, Raabe D, Zaafarani N, Zaefferer S. Acta Mater 2009;57:559.
[22] Gerberich WW, Tymiak NI, Grunlan JC, Horstemeyer MF, Baskes MI. J Appl Mech 2002;69:433.
[23] Weber F, Schestakow I, Roters F, Raabe D. Adv Eng Mater 2008;8:37.
[24] Nix WD, Gao H. J Mech Phys Solids 1998;46:411.
[25] Greer JR, Oliver WC, Nix WD. Acta Mater 2005;53:1821.
[26] Espinosa HD, Prorok BC, Peng B. J Mech Phys Sol 2004;52:667.
[27] Greer JR, Nix WD. Appl Phys 2005;80:1625.
[28] Gao H, Huang Y, Nix WD. Naturwissenschaften 1999;86:507.
[29] Parthasarathy TA, Rao SI, Dimiduk DM, Uchic MD, Trinkle DR. Scripta Mater 2007;56:313.
[30] Taupin V, Varadhan S, Fressengeas C, Beaudoin AJ, Montagnat M, Duval P. Phys Rev Lett 2007;99:155507.
[31] Gruber PA, Solenthaler C, Arzt E, Spolenak R. Acta Mater 2008;56:1876.
[32] Kiener D, Grosinger W, Dehm G, Pippan R. Acta Mater 2008;56:580.
[33] Norfleet DM, Dimiduk DM, Polasik SJ, Uchic MD, Mills MJ. Acta Mater 2008;56:2988.
[34] Maass R, Van Petegem S, Grolimund D, Van Swygenhoven H. Appl Phys Lett 2007;91:131909.
[35] Maass R, Van Petegem S, Grolimund D, Van Swygenhoven H, Kiener D, Dehm G. Appl Phys Lett 2008;92:071905.
[36] Motz C, Weygand D, Senger J, Gumbsch P. Acta Mater 2009;57:1744.
[37] Cao A, Wei Y, Mao SX. Scripta Mater 2008;59:219.
[38] Budiman AS, Han SM, Greer JR, Tamura N, Patel JR, Nix WD. Acta Mater 2008;56:602.
[39] Deshpande VS, Needleman A, Van der Giessen E. J Mech Phys Solids 2005;53:2661.
[40] Balint DS, Deshpande VS, Needleman A, Van der Giessen E. Mater Sci Eng 2006;14:409.
[41] Dehm G. Prog Mater Sci 2009;54:664.
[42] Mecking H, Lücke K. Scripta Mater 1970;4:427.
[43] Kocks UF, Mecking H. Prog Mater Sci 2003;48:171.
[44] Roters F, Raabe D, Gottstein G. Acta Mater 2000;48:4181.
[45] Hemker KJ, Nix WD. Nat Mater 2008;7:97.
[46] Afrin N, Ngan AHW. Scripta Mater 2006;54:7.
[47] Frick CP, Clark BG, Orso S, Schneider AS, Arzt E. Mater Sci Eng 2008;489:319.
[48] Zhang H, Schuster BE, Wie Q, Ramesh KT. Scripta Mater 2006;54:181.
[49] Kocks UF, Tome CN, Wenk HR. Texture and Anisotropy. Cambridge: Cambridge University Press; 1998.
[50] Maass R, Van Petegem S, Ma D, Zimmermann J, Grolimund D, Roters F, et al. Acta Mater 2009;57:5996.
[51] Maass R, Van Petegem S, Van Swygenhoven H, Derlet PM, Volkert CA, Grolimund D. Phys Rev Lett 2007;99:145505.
[52] von Blanckenhagen B, Gumbsch P, Arzt E. Model Simul Mater Sci Eng 2001;9:157.